Smart Structures and Systems, *Vol. 28, No. 4 (2021) 535-551*
https://doi.org/10.12989/sss.2021.28.4.535

Machine learning and RSM models for prediction of compressive strength of smart bio-concrete

Hassan Amer Algaifi[*1], Suhaimi Abu Bakar[**2b], Rayed Alyousef [3], Abdul Rahman Mohd. Sam [2], Ali S. Alqarni [5], M.H. Wan Ibrahim[***1c], Shahiron Shahidan[****1d], Mohammed Ibrahim [4] and Babatunde Abiodun Salami [4]

[1] *Faculty of Civil and Environmental Engineering, Universiti Tun Hussein Onn Malaysia, 86400 Parit Raja, Johor, Malaysia*
[2] *School of Civil Engineering, Faculty of Engineering, Universiti Teknologi Malaysia, Johor Bahru 81310, Malaysia*
[3] *Department of Civil Engineering, College of Engineering, Prince Sattam bin Abdulaziz University, Alkharj 11942, Saudi Arabia*
[4] *Center for Engineering Research, Research Institute, King Fahd University of Petroleum and Minerals, Dhahran 31261, Saudi Arabia*
[5] *Department of Civil Engineering, College of Engineering, King Saud University, Riyadh 11421, Saudi Arabia*

(*Received January 14, 2021, Revised April 29, 2021, Accepted June 1, 2021*)

Abstract. In recent years, bacteria-based self-healing concrete has been widely exploited to improve the compressive strength of concrete using different bacterial species. However, both the identification of the optimal involved reaction parameters and theoretical framework information are still limited. In the present study, both experimentally and numerical modelling using machine learning (ANN and ANFIS) and response surface methodology (RSM) were implemented to evaluate and optimse the evolution of bacterial concrete strength. Therefore, a total of 58 compressive strength tests of the concrete incorporating new bacterial species were designed using different concentrations of urea, cells concentration, calcium, nutrient and time. Based on the results, the compressive strength of the bacterial concrete improved by 16% due to the decrement of the pore percentage in the concrete skin; specifically, 5 mm from the concrete surface, compared to that of the control concrete. In the same context, both machine the learning and RSM models indicated that the optimal range of urea, calcium, nutrient and bacterial cells were (18-23 g/L), (150-350 mM), (1-3 g/L) and 2×10^7 cells/mL, respectively. Based on the statistical analysis, RMSE, R^2, MPE, RAE and RRSE were (0.793, 0.785), (0.985, 0.986), (1.508, 1.1), (0.11, 0.09) and (0.121, 0.12) from both the ANN and ANFIS models, respectively, while; the following values (0.839, 0.972, 1.678, 0.131 and 0.165) was obtained from RSM model, respectively. As such, it can be concluded that a high correlation and minimum error were obtained, however, machine learning models provided more accurate results compared to that of the RSM model.

Keywords: concrete strength; machine learning; response surface methodology; self-healing concrete

1. Introduction

The compressive strength of concrete is an important indicator in civil engineering (Nigdeli and Bekdas 2013, Algaifi *et al*. 2021). It is considered a key parameter that reflects the consistency and material ingredients of a concrete mix. Moreover, the compressive strength test has a direct relationship with quality and properties (Valipour *et al*. 2014, Shahmansouri *et al*. 2019). In recent years, many predictive models of concrete strength have been developed which aimed to quickly provide insight into the influential factors affecting the concrete strength and thus save cost, energy and time (Onat and Celik 2017, Nosrati *et al*. 2018, Sadowski *et al*. 2018, Muthuraj 2019, Shariati *et al*. 2020a, b, Zhao *et al*. 2020). Machine learning such as an artificial neural network (ANN) and adaptive neuro-fuzzy inference system (ANFIS) (Dutta *et al*. 2018, Shirkhani *et al*. 2019, Alabduljabbar *et al*. 2020, Ma *et al*. 2020, Perumal and Prabakaran 2020), Genetic expression programming (GEP) (Alkroosh and Sarker 2019, Nematzadeh *et al*. 2021, Shahmansouri *et al*. 2021a, b), metaheuristic algorithms (Zhao *et al*. 2021, 2021a, b), and response surface methodology (RSM) (Alshalif *et al*. 2021, Abubakar *et al*. 2018) are the most commonly used models in the literature.

For example, the compressive strength of fly ash-based concrete was predicted using ANN as the output parameter with a high degree of correlation (R^2 = 0.96) in a study by Topcu and Sarıdemir (2008). In their study, cement, water, aggregate, admixture ratio and fly ash replacement ratio were used as input parameters. Next, the strength of a high volume of fly ash-based concrete was also predicted at 28 days using ANN model in another study reported by Prasad *et al*. (2009). Similarly, an ANN model was also successfully constructed to predict geopolymer concrete with a root mean square error (RMSE) of 2.265 MPa and

*Corresponding author, Ph.D.,
E-mail: enghas78@gmail.com
**Co-corresponding author, Ph.D.,
E-mail: suhaimibakar@utm.my
***Co-corresponding author, Ph.D.,
E-mail: haziman@uthm.edu.my
****Co-corresponding author, Ph.D.,
E-mail: shahiron@uthm.edu.my

ISSN: 1738-1584 (Print), 1738-1991 (Online)

determination coefficient (R^2) of 0.879 (Dao *et al*. 2019). Sodium silicate solution, water, sodium hydroxide and fly ash were used as input variables for modelling. In the same context, GEP has gained a great deal of interest for predicting the properties of concrete such as compressive strength. For example, the high performance concrete strength was successfully estimated using GEP with minimum error and a high degree of correlation (Mousavi *et al*. 2012). Other compressive strength of cementitious materials such as lightweight concrete (Jafari and Mahini 2017) and normal concrete (Mahdinia *et al*. 2019) were also predicted using GEP method. On the other hand, RSM was also widely used in the design of concrete technology. For instance, Soto-Pérez *et al*. (2015) investigated the influential factors that affect the compressive strength such as water-to-binder ratio, nano-iron oxide content and fly ash content. In the same context, the evolution of compressive strength of recycled concrete aggregates with different range of slump and cement was also evaluated and compared using RMS and ANN models (Hammoudi *et al*. 2019). According to their results, it was found that the developed ANN model shows better accuracy compared to that of the RSM model.

From another point of view, mathematical models for compressive strength of bacteria concrete are very limited in the literature. In particular, there is not yet a predictive model or codal provisions for determining the bacterial concrete strength and their involved parameters such as urea, calcium and bacterial cells concentration. However, a lot of experimental works were carried out to obtain the compressive strength of bacterial concrete incorporating different bacterial species (Algaifi *et al*. 2018, 2020). For example, Nain *et al*. (2019) found an improvement in the concrete compressive strength by 14.36%, 22.58% with the incorporation of *B*. subtiltis and *B*. megaterium, respectively, compared to the conventional concrete specimens. The improvement in concrete strength was attributed to the production of microbial calcium carbonate, which acted as a sealant and led to better packing inside the cement-based matrix. Similar results were demonstrated by Reddy and Revathi (2019), who attained an increase of 20% in concrete strength with the incorporation of *B*. Sphaericus (10^5 cells/mL). Similarly, the maximum improvement value of concrete strength was found at 10^5 cells/mL using *B*. subtiltis (Jena *et al*. 2020). On the other hand, Su *et al*. (2019) indicated that concrete strength increased at a bacterial cell concentration of 10^{13} cells/mL. Furthermore, the authors also recorded a reduction in concrete strength at 10^{14} cells/mL. Other published research, in terms of the effect of bacteria on concrete strength or durability aspect, are available in the present literature (Mondal and Ghosh 2019, Nguyen *et al*. 2019, Shaheen *et al*. 2019, Jakubovskis *et al*. 2020, Nathaniel *et al*. 2020, Wu *et al*. 2020).

Considering the above, it can be inferred that the theoretical modelling of compressive strength of bacterial concrete prediction is still limited. Hence, in the present study, machine learning and RSM were utilised to develop a new predictive model to assess the bacterial concrete strength and the involved parameters using new bacterial species. To achieve the goal of this study, 58 experimental tests were conducted to examine the compressive strength of bacterial concrete under different concentrations of bacterial cells (5×10^6 – 2×10^7 cells/mL), urea (5 - 30 g/L), calcium (100 – 500 mM), yeast extract (1 – 20 g/L) and time (7, 14 and 28 days). In addition, X-rays CT scan was utlised to assess the evolution of the bacterial concrete microstructure. Moreover, several statistics indicators were also used to evaluate and compare the accuracy between the developed models and experimental data. The present research would significantly contribute to the self-healing research progress in developing a guideline to optimize influencing parameters on the concrete strength. Furthermore, this study addressed and clarified how the bacteria could significantly improve the interfacial transition zone (ITZ) and pore structures to better understand the bacterial activity inside the concrete matrix in future studies before the real application in the industry. Moreover, the predicted models also helped the researchers to minimize both cost and time during the experimental works.

2. Materials and methods

2.1 Proportions of the control concrete mix

Cement Portland type (I) comply with the specification of American Society for Testing and Materials C150 (2004) was used in the present study. In addition, natural sand was utilised as fine aggregate with a nominal size of 4 mm, while, the coarse aggregate was crushed from granite with a maximum size of 10 mm complying with BS 882: 1992 specification. The specific gravity of both fine and coarse aggregate were 2.6 and 2.7 respectively. To enhance the workability of concrete, Rheobuild 1100 superplasticising was added (1% of cement weight) into the mixing water. The characteristic compressive strength of the concrete was 30 MPa after 28 days. The mix proportions of the control concrete were designed and calculated according to the standard British method (DOE). In particular, the output of the concrete proportions was 235 L/m^3 water, 425 kg/m^3 cement, 618 Kg/m^3 granite type 10 mm aggregates and 1098 kg/m^3 natural sand. In addition, the target mean strength was found to be 36.5 MPa at water cement ratio of 0.55 and a slump of 160 mm.

2.2 Preparation of the bacterial concrete mix

2.2.1 Bacterial strain and initial screening

New bacterial species was used to achieve the aim of the present study. It was isolated from soil at Universiti Teknologi Malaysia (UTM) grounds. In addition, the partial sequence of the DNA (16S rRNA) of the isolate bacteria was identified and deposited in the National Centre for Biotechnology Information (NCBI) databases under name of *Bacillus* pseudomycoides strain HASS3 and accession numbers of MK357893. After that, the ability of the bacteria to hydrolyse urea and induce calcium carbonate was also tested to ensure that the isolate bacteria had the ability to induce ureases enzyme. Urease enzyme is

regarded as the main sole factor to hydrolyse urea into qhrqncarbonate. Such carbonate reacts with calcium to produce calcium carbonate. In particular, the hydrolysis of urea was evaluated using the Nessler Method 8038. This was achieved by culturing the isolate bacteria in a 100 mL flask, which was filled with 30 mL Lysogeny broth (LB), 6 mM urea and 2 mM calcium chloride. Subsequently, it was incubated for 24 h at 37°C. In the next step, the bacterial culture (0.1 mL) was taken out and centrifuged to measure the concentration of ammonia (NH_3). This process was carried out in the Centre for Water Security (IPASA-UTM) and Environmental Sustainability. Later, a 50 mL centrifuge tube was filled up with 25 mL distilled water to dilute the bacterial solution. Following that, three drops of polyvinyl and mineral stabiliser (each) were added into the solution. Later on, using a pipette, 1 mL Nessler reagent was taken and mixed into the solution for one minute. Subsequently, 10 ml of the solution was transferred to the targeted cuvette in the UV-Vis spectrophotometer (Hach, DR5000 Model), which measured the amount of ammonia in the solution (mg/L). The amount of ammonia and its presence would indicate the isolate bacteria's ability to produce urease enzyme. This is because urease enzyme is responsible for the decomposition of urea into ammonia and carbonate. It should be noted that the amount of ammonia was calculated using Eq. (1) (Wang *et al*. 2017).

$$ureahydrolysis_{(mg/L)} = \frac{NH_3^+{}_{(mg/L)} \times 60_{(g/mole)}}{2 \times 17_{(g/mole)}} \quad (1)$$

Finally, the precipitation of microbial calcium carbonate was identified using X-ray diffraction (XRD), while the morphology of the bacteria was examined, before and after precipitation, using variable pressure scanning electron microscope (VP-SEM). Several steps were taken to examine the morphology of the bacteria cell. Firstly, the bacterial culture (30 mL) was incubated overnight, followed by centrifuging. Then, the harvested bacterial cells were washed in a microcentrifuge tube (2 mL) filled with distilled water (dH_2O). Later, the bacterial cells were transferred and added to a cover glass (Fisher Scientific). To facilitate the adhesion between the glass and cells, the glass was coated with poly-lysine, prior to the addition of the bacteria. In a similar concept, to fix the bacterial cells to the glass, 1 mL of 2.5% glutaraldehyde solution was also added to the glass. After that, the target spot was immersed in hexamethyldisilazane for 2 hours. Then, the glass was kept in a desiccator overnight to ensure the complete drying of the bacterial cells. Finally, the target spot was examined via VP-SEM after both coating and dehydrating in order to increase the quality of the image resolution.

To identify the microbial precipitation product, 30 mL LB with the inclusion of urea-$CaC1_2$ was incubated (Infors HT Ecotron incubator) for 7 days, as described in Fig. 1(a). Next, the centrifugation (KUBOTA, 5922 Model) of the bacteria culture was carried out for 10 min. at 10000 rpm, as illustrated in Fig. 1(b). Subsequently, referring to Fig. 1(c), the precipitated product was placed in an oven for 24 h at 60°C for drying purposes. Finally, based on Fig. 1(d), the precipitated crystal was collected and ground into fine powder. The said fine powder was then examined using XRD, which is commonly used to identify crystal material. This technique is executed by recognising both the atomic layer spacing (d) and atom arrangement (structure of crystals), which are distinctive for every solid material (Scrivener *et al*. 2004). In particular, the SmartLab X-rays diffractometer (Rigoku) was used to identify the microbial product. To produce intensive X-rays spectra (CuKa radiation = 1.5418Å), the test was operated at 40 kV and 30 mA with Cu anode. In addition, D/teX Ultra 250 detector over Bragg angle (2 theta3 - 100), 8.2551 deg/min, 0.0200 deg /step as continuous scans for 10 min.) were used to collect the diffracted patterns.

2.2.2 Bacterial spore solution

The isolate bacteria were overnight grown in a 100 mL flask filled with 30 mL of lysogeny broth under shaking (150 rpm) at 37°C. It is interesting to note that a 0.01 g/L of $MnSO_4.H_2O$ was added into the bacterial culture in order to form the bacterial spores. Based on the recommendation of Wang *et al*. (2017), the bacterial culture should be incubated for two weeks to ensure that at least 90% of the vegetative cells are converted into spores.

After that, the bacterial culture was centrifuged for 4 mins at 5,000 rpm. Then, the deposited spores were suspended in saline solution and kept in a cooling room (4°C) for further use with a concentration of 10^9 cells/mL

(a) Incubation (b) Centrifuging (c) Drying (d) Grinding

Fig. 1 Preparation process for the XRD

It should be noted that the concentration of the bacteria was calculated using a spectrophotometer (Jenway 7305 UV/Visible) at OD600 and Eq. (2). Where N was the value of the obtained optical density OD_{600} and Q denoted the bacterial cells.

$$Q = 8.59 \times 10^7 N^{1.3627} \quad (2)$$

2.2.3 Concrete strength test

The bacterial concrete mix was designed in a similar manner of the control mix. However, different concentration of urea (5 g/L – 20 g/L), calcium nitrate tetrahydrate (100 mM – 500 Mm), bacterial cells (5×10^6 – 2×10^7 cells/mL) and yeast extract as nutrient (1 – 20 g/L) were added during the concrete mixing in order to implement the ureolytic activity inside the concrete matrix. In particular, the bacterial spore solution was replaced by a part of mixing water using the dilution equation Eq. (3). Where C_2 was the bacterial cells concentration of the new solution and V_2 indicated the volume of the new solution. Moreover, C_1 was the concentration of the stock solution and V_1 represented the stock solution volume. On the other hand, the urea, calcium nitrate tetrahydrate and nutrient were added into the mixing water using the morality formula as shown in Eq. (4).

$$C_1 \times V_1 = C_2 \times V_2 \quad (3)$$

$$\text{Molarity}(M) = \frac{\text{weight}_{(g)}}{\text{volume}_{(L)} \times \text{molarmass}_{(g/M)}} \quad (4)$$

After that, cubes of 100×100×100 mm in size were cast and cured in a water tank. Then, they were tested at different ages (7, 14 and 28 days), as per BS EN 12390-3:2009. Both control and bacterial concrete specimens were assessed in triplicate. After 24 h of casting, the specimens were demoulded and cured in a water tank at room temperature (28 ± 2°C) until the specimens were tested. The compression testing machine (NL Scientific) with a capacity of 3000 kN was utilised to conduct the compressive strength test, as per BS 1881 part 116 (1983).

2.2.4 Concrete microstructure

In recent years, X-rays micro-computed tomography (X-rays μCT) has gained a positive standing in the applications of engineering, specifically, regarding material porosity (Snoeck *et al*. 2016, Mahmud *et al*. 2017, Sokhansefat *et al*. 2020). In the present study, the the concrete microstructure was examined at Universiti Teknologi Petronas (UTP) using X-rays μCT (Inspexio SMX-225 CT, Shimadzu, Japan). To achieve the target resolution, a small mm-sized of the mortar was prepared and taken into account to represent the concrete matrix based on BS EN 196-1:1995. In particular, the ratio of cement to sand was 1:3 by mass and the water cement ratio was kept constant at 0.6. In addition, the optimum concentration of urea (20 g/L), calcium nitrate tetrahydrate (250 mM), nutrient (3g/L) and bacterial cells (2×10^7 cells/mL) were added during the mortar mixing. Then, mortar specimens (Φ10, 20 mm and Φ25× 40 mm) were cast. After 2h hours, the mortar specimens were cured in tap water and kept for 28 days in order to carry out the X-rays test.

After that, the target sample was placed between the X-ray source and an X-ray detector. Then, the emitted X-rays travelled towards the detector through the cross-section of the sample, relying on the density of the material. In particular, the intensity of the pass X-rays was converted into the grey level from 0 to 255. The higher density was represented by light grey level value, whereas the higher value of grey level reflected the porous material. In the present study, the output voltage was raised up to 130 kV with the ampere of 100 mA to obtain high quality images. In addition, to improve details and resolution, the sample was rotated at 360° to create projections. Subsequently, 3D constructed slices were developed by VGStudio Max 3D rendering program. Finally, to observe and analyse the porosity and ITZ, myvgl33 reader software was used.

2.3 Mathematical models

2.3.1 Response surface methodology

Response surface methodology (RSM) is one of the most commonly used predicted approach in the field of civil engineering (Kathirvel and Kaliyaperumal 2017, Shahmansouri *et al*. 2021a, b). It involves the combination of both statistical and mathematical methods to assess the relationship between the independent variables (influential factors) and dependent variables (response). In the present study, five influential factors (X_i) were represented by concentration of bacterial spores, urea, nutrient, calcium and time. While, the compressive strength of the bacterial concrete acted as one response (Y). In particular, forty-eight compressive strength tests were imported and analysed through the historical data tool of the Design expert software. In addition, the limit, codes and unit of the five influential factors are shown in Table 1. In other words, the maximum applicable limit of the involved parameters was adopted in the present study. For example, it is believed that improved bacterial concrete strength is achieved at an early age, specifically at the first four weeks (Algaifi *et al*. 2020). This is because the contribution of the bacteria to improve strength is very limited at a later age. In particular, the bacteria would not induce calcium carbonate later due to improved concrete microstructure over time, discussed in detail in section 3.2.

In the same context, second order polynomial equation was taken into account to estimate the response as well as show the relationship of the influential factors as shown in Eq. (5). where, βo and β_i are regarded as a constant and linear coefficient. In addition, βii and β_{ij} represented the

Table 1 Codes and limit of the influential factors

Influential factors	Code	Unit	Limit	
			Minimum	Maximum
Bacterial cells	X_1	Cells/mL	5×10^6	2×10^7
Urea concentration	X_2	g/L	5	30
Calcium concentration	X_3	mM	100	500
Nutrient concentration	X_4	g/L	1	20
Time	X_4	days	7	28

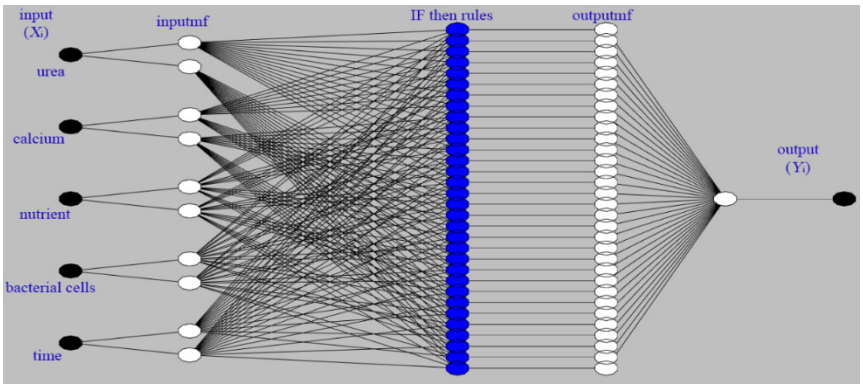

Fig. 2 Structure of proposed ANFIS model

quadratic and interactive coefficients.

$$Y = \beta_o + \sum_{i}^{k} \beta_i X_i + \sum_{i}^{k} \beta_{ii} X_i^2 + \sum_{ij}^{k} \beta_{ij} X_{ij} \quad (5)$$

2.3.2 Adaptive neuro-fuzzy inference system

Besides the fact that the ANN was recognised as an efficient and robust technique in many civil engineering application, Adaptive Neuro-Fuzzy Inference System (ANFIS) was also found to be a better method when the relationship between the input and output is very complicated (Golafshani *et al*. 2020, Naderpour and Mirrashid 2020, Huseien *et al*. 2021). This is because ANFIS combined the advantages of both fuzzy inference system (FIS) and ANN, which enable them to deal with nonlinear and complicated problems (Al-Mughanam *et al*. 2020, Alabduljabbar *et al*. 2020, Golafshani *et al*. 2020, Shariati *et al*. 2020a, b). Therefore, in the present study, both ANN and ANFIS were, separately, utilised to predict the evolution of bacterial concrete strength and the involved parameters. The efficiency of the proposed ANFIS and ANN models were compared and evaluated using different statistical validation methods.

In fact, ANFIS mimic the human behaviors of human by involving 'If–then rules'. For simplicity, two input parameters (X_1, X_2) and one output (Y_1) were taken into account in order to briefly explained the process of ANFIS. The framework and process of ANFIS consist of several steps or layers namely, input layer, fuzzifaction, rules, normalization, fuzzy inference and defuzzifaction layer. The input layer consists of fixed neurons which represent the value of the real data. Then, the second one is fuzzication layer which involves adapting neurons. In this layer, the fuzzy set of the input later is calculated using the suitable membership function as shown in Eqs. (6) and (7).

$$O_i^2 = \mu A_i(x_1) \quad (6)$$

$$O_i^2 = \mu B_i(x_2) \quad (7)$$

Where, μAi and μBi are the target membership. Indeed, there are several membership functions such as Gaussian function, triangular, sigmoid, etc. For example, if a sigmoid function is considered, then μAi is measured by Eq. (8) in which a and b are parameter set.

$$\mu A_i = \frac{1}{1 + e^{-a(x-b)}} \quad (8)$$

For the same regard, the firing layer represents the third layer in which the output firing strength (output) w_i, is calculated by multiplied the output of the second layer as shown in Eq. (9). It is intestine to note that the neuron of this layer is fixed neurons.

$$w_i = \mu A_i(X_1) \times \mu B_i(X_2) \quad (9)$$

In addition, the fourth layer is known as the normalisation layer involving fixed neurons that receive the firing strength and normalize them. In particular, the firing strength for each node is divided by the sum of all the fire strength of the rule layer as shown in Eq. (10).

$$\overline{w_i} = \frac{w_i}{\sum w_i} \quad (10)$$

Moreover, the fifth layer represent the If-then rules in which the output of the normalization layer was multiplied by either zero or first order polynomial equation (f_i) as shown in Eq. (11). This process is called the defuzzification layer. Where a, b and c are the parameters set in the consequence function.

$$O_i^5 = \overline{w_i} f_i \quad (11)$$

For example, if first order polynomial (linear equation) was considered then, the If-then rules are represented as follows:

Rule1: if X_1 is A_1 and X_2 is B_1 then f_1=p_1 X_1+q_1 X_2+r_1
Rule2: if X_1 is A_2 and X_2 is B_2 then f_1=p_2 X_1+q_2 X_2+r_2

Where p_i, q_i and r_i are the obtained parameters during the training process.

Finally, the sum of defuzzification output was calculated in the six layers as shown in Eq, (12). It is interesting to note that the neuron in this layer is fixed neurons.

$$O_i^6 = \sum \overline{w_i}. f_i \quad (12)$$

From the viewpoint of the proposed ANFIS model, five

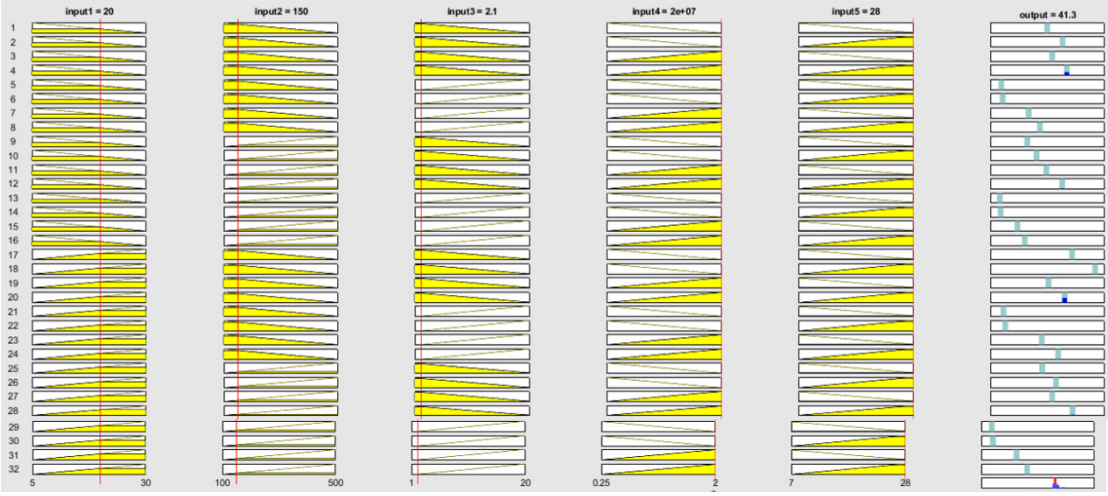

Fig. 3 Fuzzy inference diagram for the developed ANFIS model

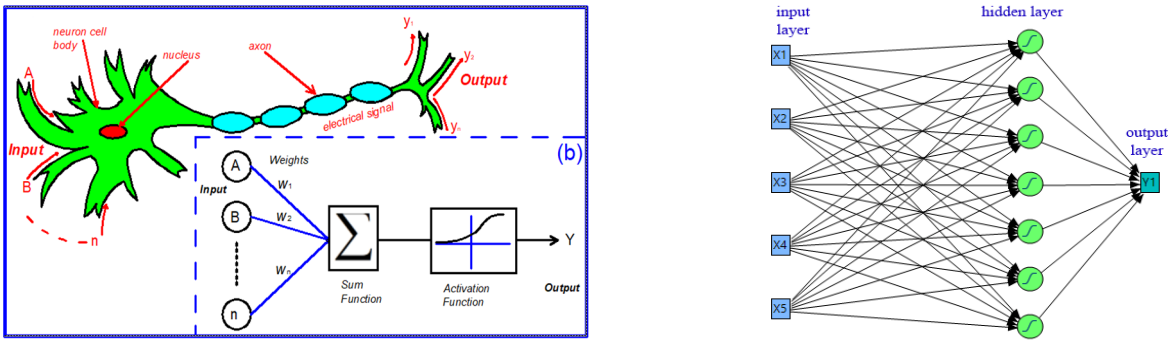

(a) Function of human brain (b) Artificial neural network

Fig. 4 Neural network processing

input parameters (x_i), including urea, calcium, nutrient, bacterial cell concentration and time, were considered to construct the model, as shown in Fig. 2. Then, a triangular membership function (trimf) was adopted for fuzzification of the target input parameters (inputmf) and the output of the fuzzy if-then rules (outputmf) was obtained using a zero-degree polynomial equation (constant). In particular, a total of 25 rules was constructed for the present ANFIS model. For example, Fig. 3 presents the diagram of the fuzzy inference approach for the input vector (20, 150, 2.5, 2e07, 28). The vector represents the value of urea, calcium, nutrient, bacterial cell concentration and time, respectively. It is interesting to note that 48 and 10 experimental tests were carried out and taken for training and validation purposes. In addition, the MATLAB ANFIS toolbox was utlised to construct the model.

2.3.3 Artificial neural network (ANN) Model

Artificial Neural Network (ANN) is also one of the most biologically inspired computational models in civil engineering application (Shahmansouri *et al*. 2020, Nematzadeh *et al*. 2021). It simulates the information process of the human brain as shown in Fig. 4(a). The human brain contains billions of neurons which are interconnected by axons. The neuron processes the information in the form of an electrical signal in three steps receiving, processing and recognition. In the receiving step, neuron dendrites receive the external information and proceed it in the cell of neuron as a chemical signal. With a sufficient amount of chemical signals inside the neuron cell, an electrical signal is generated which is termed as the processing step. These electrical signals are then passed to the next neuron through an axon path. Then, in the recognition step, the next neuron has to decide (on its own) either to reject or accept them according to the strength of the electrical signal. Similarly, an ANN is composed of several artificial neurons to mimic the actual biological neuron function. First, the receiving information (input values) are weighted and combined via an activation function. Then, these input values are passed and processed inside the neuron through a mathematical transfer activation function. Subsequently, the output reflects the behaviour of the neuron in a manner similar to the electrical signal of the actual neuron. This is demonstrated in Fig. 4(b).

In the present study, the developed model consists of three layers as shown in Fig. 4(c). The first layer namely input later (I) contains five neurons (parameters) which are represented by urea, calcium, yeast extract, bacterial cells concentration and time. Then, seven neurons of the hidden layer (H) were used to achieve the best performing model which is consistent with Bahiraei *et al*. (2020), who found that one hidden with seven neurons was the best case to

develop an ANN model using 34 data samples. Similarly, Liu *et al*. (2021) stated that small numbers of hidden layers and neurons are good choices to avoid overfitting the data.

In addition, one neuron in the third layer was used to reflects the predicted compressive strength of bio-concrete namely output layer (O). It is interesting to note that a total of 58 experimental test (80% for training and 20% for validation purposes) were utilised to construct the proposed ANN model using JMP software. Moreover, the TanH sigmoid function was adopted to map the input with the target output using Eq. (13).

$$f_{(x)} = \frac{e^{2x} - 1}{e^{2x} + 1} \tag{13}$$

2.4 Validation of the models

In the present study, the performance of both techniques ANN and RSM were evaluated using different statistical indicators. For example, the residual, mean square error (MSE) and root mean square error (RMSE) were used as an estimator in the statistical terms. They were considered to quantify the degree of difference between the actual value of the experimental results and the predicted compressive strength of concrete. In particular, when the value was close to zero, the disparity between both the actual and predicted output achieved minimal. In addition, with a smaller value of error, a more efficient model can be achieved is obtained. The MSE and RMSE formula are expressed as shown in Eqs. (14) and (15). Where Y_A was the experimental result of the concrete strength and Y_P was the predicted concrete strength from the model.

$$MES = \frac{1}{N}\sum_{i=1}^{N}(Y_P - Y_A)^2 \tag{14}$$

$$RMES = \sqrt{\frac{1}{N}\sum_{i=1}^{N}(Y_P - Y_A)^2} \tag{15}$$

In the same context, determination coefficient (R^2), adjusted R^2 and R was also taken into account as a statically estimator. In particular, it was utilised to evaluate the strength of the results. In addition, both R^2 and adjusted R^2 are able to provide insight into the degree of fitting between the network output and the collected experimental data as expressed in Eqs. (16) and (17). Where the average value of the predicted results was termed as Y_{Pmean}, whereas, the number of experimental runs was represented by N. Moreover, the best fitting of actual compressive strength of the bio-concrete and the predicted results is accrued by increasing the value of the determination coefficient. Its value is also normally in the range of 0–1. Where N is the number of the experimental test and K is the number of the influential factors.

$$R^2 = \frac{\sum_{i=1}^{N}\left(Y_A - Y_{A_{mean}}\right)^2 - \sum_{i=1}^{N}(Y_A - Y_P)^2}{\sum_{i=1}^{N}\left(Y_A - Y_{A_{mean}}\right)^2} \tag{16}$$

$$R^2_{adj} = 1 - \left[(1 - R^2) \times \frac{N-1}{N-K-1}\right] \tag{17}$$

In addition, the mean percentage error (MPE) (Awolusi *et al*. 2019) was used for analysing the efficiency of the developed model as shown in Eq. (18) receptively. MPE is also necessary in order to assess the accuracy of the proposed model.

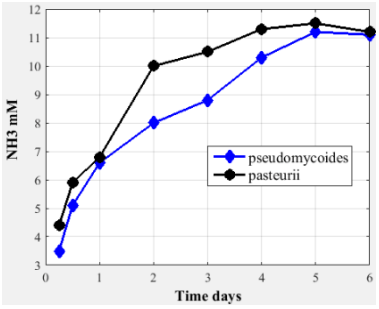

(a) Urease activity

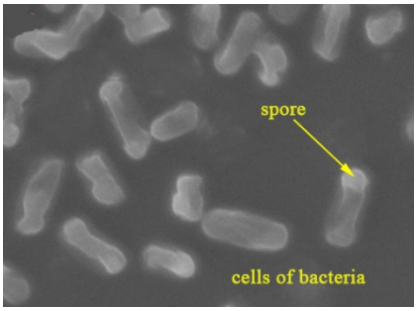

(b) Cell morphology before precipitation

(c) Cell morphology after $CaCO_3$ precipitation

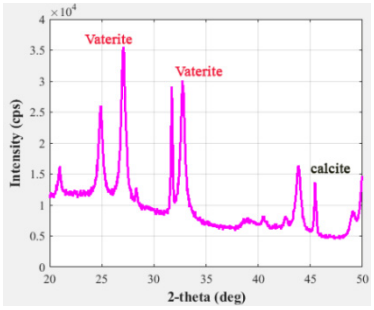

(d) Identification of the microbial product by XRD

Fig. 5 Initial screening of the isolated bacteria

$$MPE = \left(\frac{100}{N}\sum_{i=1}^{N}\left|\frac{Y_A - Y_P}{Y_p}\right|\right) \quad (18)$$

Moreover, other statistical indicators were also utilised to prove the performance of the model such as Relative Absolute Error (RAE) Eq. (19), Mean Root Relative Squared error (RRSE) Eq. (20) and Correlation Coefficient (R) Eq. (21) (Altowayti *et al*. 2019). These indicators also aimed to assess the error, differences and correlation between the predicted and actual results.

$$RAE = \frac{\sum|(Y_P - Y_A)|}{\sum\left|\left(Y_P - \frac{1}{N}\sum Y_A\right)\right|} \quad (19)$$

$$RRSE = \sqrt{\frac{\sum(Y_P - Y_A)^2}{\sum\left(Y_P - \frac{1}{N}\sum Y_A\right)^2}} \quad (20)$$

$$R = \frac{(N\sum Y_A Y_P - \sum Y_A \sum Y_P)^2}{(N\sum Y_A^2 - (\sum Y_A)^2)(N\sum Y_P^2 - (\sum Y_P)^2)} \quad (21)$$

3. Results and discussion

3.1 Initial screening of the isolate bacteria

Based on the results, the isolate bacteria proved its ability to induce urease enzyme, which is the main sole parameter to hydrolyse urea into carbonate. As expressed in Eq. (22), carbonate ions would react with the calcium that is available inside the concrete matrix to produce calcium carbonate.

$$CO(NH_2)_2 + 2H_2O + Ca^{2+} \xrightarrow{urease} 2NH_4^+ + CaCO_3 \quad (22)$$

In addition, the hydrolysis efficiency of the isolate bacteria was evaluated by comparing its productivity with another bacterial species namely, *S*. pasteurii ATCC 11859. *S*. pasteurii ATCC 11859 was obtained from Bio-Focus Saintifik Sdn Bhd. in order to compare and assess the efficiency of the isolate bacteria as the *S*. pasteurii species has been regarded as one of the most commonly used bacterial species in the field of bio-based self-healing concrete (Bundur *et al*. 2017). Fig. 5(a) show that both bacterial species were able to hydrolyse urea into carbonate and ammonia at an almost similar rate. From the point of bacterial morphology, it could be seen that the isolate bacteria was rod shaped, in which its length and width were 4 µm and 1 µm respectively as shown in Fig. 5(b).

On the other hand, after the precipitation of calcium carbonate on the bacterial cells, its size was bigger which is also known as bacterial aggregate (40–50 µm) as illustrated in Fig. 5(c). Accordingly, the formation of bacterial aggregate required several steps. Firstly, the calcium ion stacked on the cells surface of the bacteria. After that, the chemical reaction between both the calcium and carbonate began to deposit as small crystals. Then, the small crystals bonded with each other to form a big crystal, which is also known as bacterial aggregate. In the same context, the microbial $CaCO_3$ was identified as both vaterite and calcite, as shown in Fig. 5(d) in which the amount of vaterite was higher than calcite. This was in a good agreement with previous studies. For example, Qian *et al*. (2009) concluded that the microbial $CaCO_3$ product induced by Bacillus Pasteurii was identified as calcite (predominantly) and small quantities of vaterite.

3.2 The optimum concentration of the affected parameters

The optimum value of the influential parameter on bacterial concrete strength were obtained and discussed. Based on the numerical optimization technique of RSM model (Fig. 6(a)), it can be seen that optimum compressive strength of bacterial concrete was achieved with urea concentration of almost 20 g/L, calcium concentration of

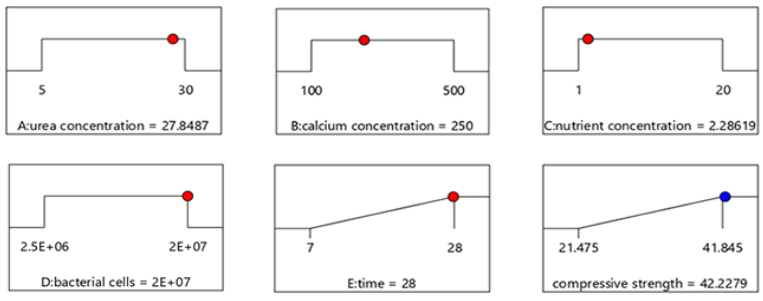

(a) RSM model

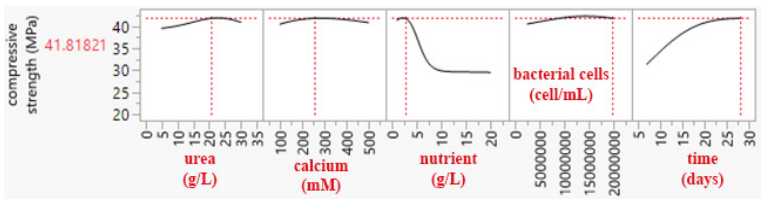

(b) ANN model

Fig. 6 Optimization of the affecting parameters

250 mM, low concentration of nutrient (close to 3 g/L) and maximum bacterial cells concentration (2×107 cells/mL). This finding is in line with the predicted optimum value using the neural network model, as shown in Fig. 6(b).

In the same context, the optimum range of the affecting parameters can also be observed via 3D plot of ANN model. It can be seen that the maximum bacterial concrete strength was obtained at a concentration of urea (18 – 23 g/L) as shown in Fig. 7(a). In addition, Fig. 7(b) shows that calcium concentration from 200 mM to 250 Mm was found to be the optimum range to enhance the strength. In contrast, strength improvement was accompanied by low nutrient concentration (less than 3 g/L), as shown in Fig. 7(c). While increasing the bacterial cell concentration up to 2×10 cell/mL leads to an increase in the compressive strength, as shown in Fig. 7(d).

These outcomes are also consistent with the predicted results from RSM and ANFIS models. For example, Fig. 8 presents the color distribution of the bacterial concrete strength gain using both response surface 3D plot (RSM model) and counter plot (ANFIS model). In particulate red color regain represents the highest compressive strength, while, the blue color zone represents the lowest strength gain. Based on the results, it can be seen that the highest strength was achieved at an optimum concentration of urea (333 mM), calcium (250 mM), yeast extract (3 g/L) and bacterial spores (2×10^7 cells/ml).

For example, Figs. 8(a) and (b) show the evolution of bacterial compressive strength over time by varying urea concentration from 5 to 30 g/L and at a fixed concentration of calcium (250 mM), nutrient (3 g/L) and bacterial cells (2×10^7 cells/mL). It is observed that the strength improved with an increase in the urea concentration. This is because urea is regarded as a source of carbonate ions in which the bacterial cells decompose urea into carbonate and ammonia. With more carbonate ions, more calcium carbonate would precipitate. This fact is consistent with Balam *et al*. (2017) who linked the strength enhancement with the available amount of urea. In addition, it can be seen that the optimum value of urea concentration to obtain the maximum concrete strength was identified as 20 g/L. Beyond the said amount, no significant changes in concrete strength were observed. This was because the bacteria had a limited capacity to hydrolyse urea. Given that, the amount of urea concentration should be used prudently so as to not affect the cost.

Similarly, the effect of calcium on the bacterial concrete strength was also investigated by varying calcium dosage from 20 to 500 mM and optimum concentration of urea, nutrient and bacterial cells as shown in Figs. 8(c) and (d). The enhancement of concrete strength regain is located where the calcium concentration ranges from 150-350 mM. However, it can be inferred that the optimum cost-effect concentration was 250 mm. Beyond this value, the strength enhancement is not significant. This is because the excessive amount of calcium is not important for bacterial activity, based to Zhang *et al*. (2016), when calcium concentration was greater than 60 mM, both ureolytic

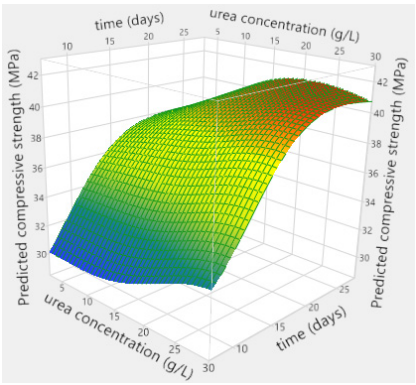

(a) Urea and time

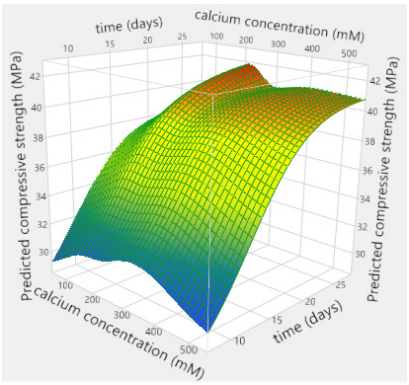

(b) Calcium and time

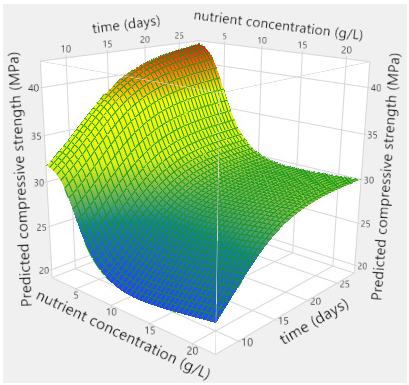

(c) Nutrient and time

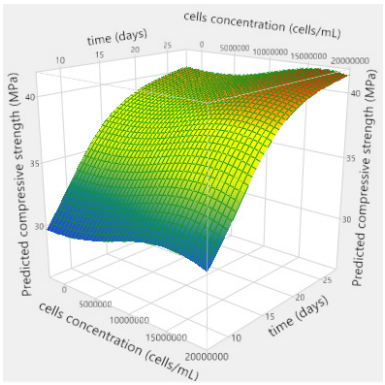

(d) Bacterial cells and time

Fig. 7 Evolution of the predicted bacterial concrete strength using ANN model as a function of time and any of the input parameters

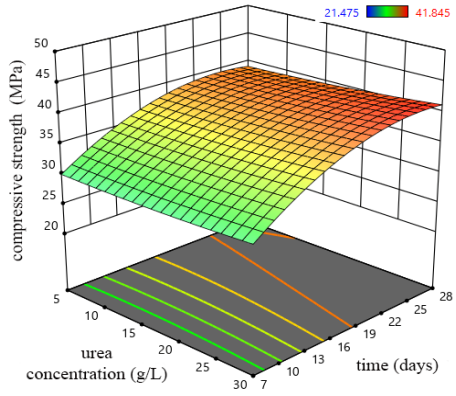

(a) Urea and time RSM model

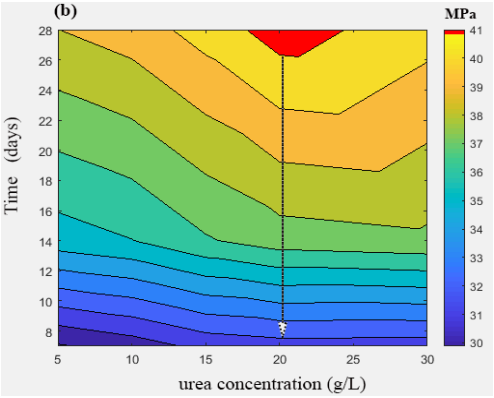

(b) Urea and time NAFIS model

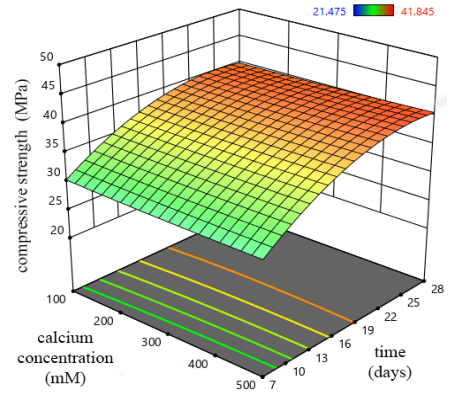

(c) Calcium and time RSM modeli

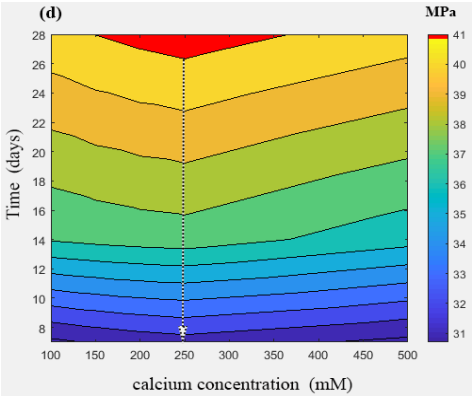

(d) Calcium and time ANFIS model

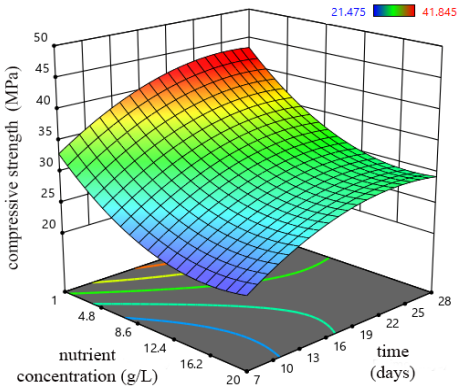

(e) Nutrient and time RSM model

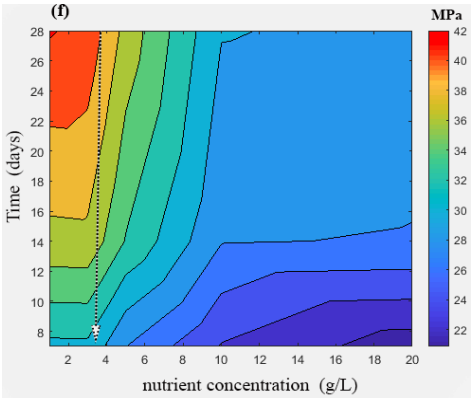

(f) Nutrient and time ANFIS model

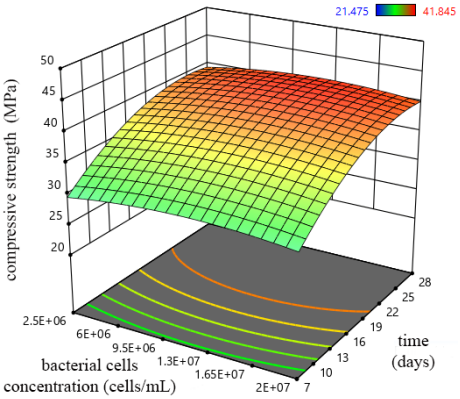

(g) Bacterial cells and time RSM model

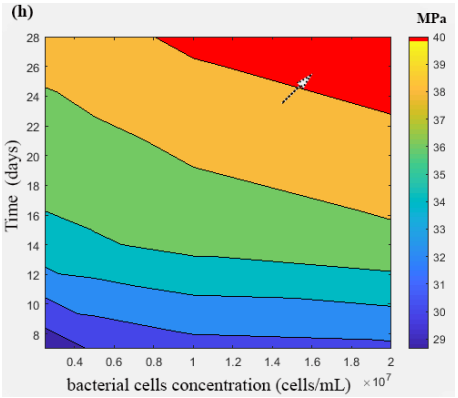

(h) Bacterial cells and time ANFIS model

Fig. 8 Evolution of the predicted bacterial concrete strength using RSM and ANFIS models as a function of time and any of the input parameters

activity and bacterial growth were negatively affected.

On the other hand, it is found that bacterial cell concentration plays a great role in the productivity rate of microbial calcium carbonate precipitation. It is interesting to note that the concomitant increase in bacterial cells concentration significantly enhanced the concrete strength as shown in Figs. 8(g) and (h). This owed to the presence of bacterial cells, which in turn, could have filled the pores or any defect in the cement-based environment due to several main reasons. In particular, the bacterial cells might fill any micro-voids inside the concrete matrix, even without any precipitation of calcium carbonate. This finding was consistent with a previous study by Su *et al*. (2019). In addition, the bacterial cells acted as a nucleation site for the deposition of microbial $CaCO_3$ product. This was due to the differences in electrical charge between both the bacterial cells and calcium ions. As such, as more bacterial cells were present, more calcium carbonate formed. Moreover, the bacterial cells were essential for $CaCO_3$ precipitation through the production of urease enzyme. Given that, without the bacteria cells, the urea could not be hydrolysed into carbonate ions, which would later react with calcium to form $CaCO_3$ at the surface of the cell. Therefore, it could be concluded that the bacterial cells are important in order to create a bacterial aggregate, which is responsible for plugging the capillary pores or cracks in the matrix. This fact was in line with previous studies who used different bacterial species. For example, Okwadha and Li (2010) concluded that the amount of calcium carbonate deposition was linked to a higher concentration of bacteria cells. Another study stated that the precipitation of microbial calcium carbonate was found in enhanced concrete strength by filling the pores of the concrete as well as the microcracks in the concrete matrix using another Bacillus bacterial species (Siddique *et al*. 2017).

In contrast, the nutrient concentration did not play a significant role in the enhancement of concrete strength. In addition, the excessive amount of calcium and yeast extract negatively affected the compressive strength of the concrete. This is because the concentration of yeast extract inside the concrete matrix might hinder and affect the process of hydration chemical reaction. Figs. 8(e) and (f) presents the relation between the yeast extract concentration value and concrete strength. It was demonstrated that there was a slight improvement in the compressive strength when the yeast extract concentration was lower than 3 g/L. Moreover, a significant decline in compressive strength was also observed when the yeast extract concentration was greater than 5 g/L. Similar findings were also observed by Bundur *et al*. (2015), who were on the view that the addition of 20 g/L yeast extract had a negative influence on concrete strength.

In general, it can be inferred that the maximum bacterial concrete strength was found to be 41.85 MPa at the optimum concentration of the affecting parameters. In addition, it was 16% higher than the control mix (36.5 MPa) after 28 days. The increase in the compressive strength at all ages was attributed to the improvement of the concrete microstructure. In particular, the isolate bacteria decomposed the urea into carbonate, which then reacted with the available calcium to produce both vaterite and calcite as discussed earlier. As a result, both vaterite and calcite filled the pores and defects, which then densified the microstructure of the concrete. Fig. 9 shows a 2D cross-section of the bacterial concrete specimen which was obtained using X-rays CT scan. It was aimed to observe and analyse the porosity of the concrete with and without bacteria.

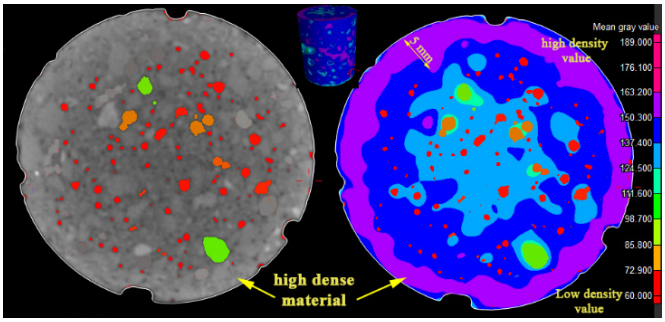

(a) Bacterial concrete specimen

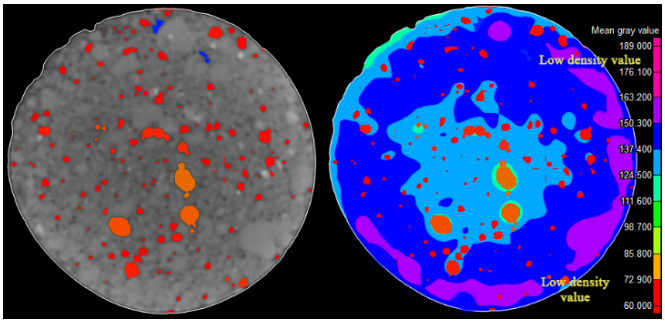

(b) Control concrete specimen

Fig. 9 Distribution of the pores

In general, the concrete specimen observed the generated X-rays according to its density and compositions in the form of digit numbers (i.e., pixel images). For example, the porous concrete absorbed less X-rays. As such, the detector received a high amount of the X-rays which was converted to the maximum grey level (dark

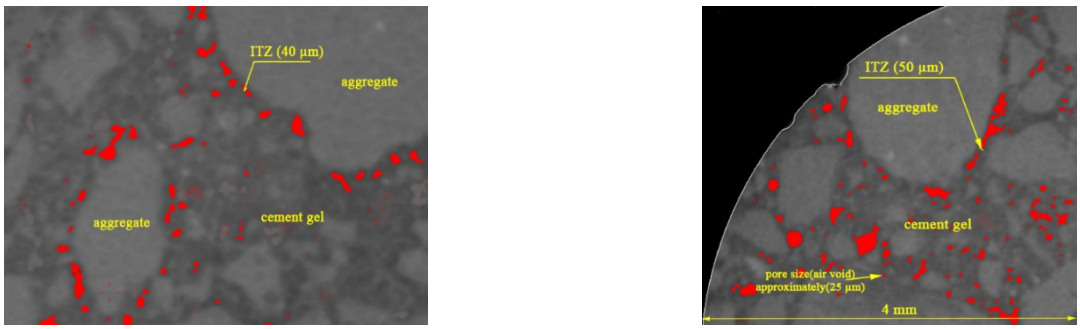

(a) Bacterial concrete specimen (b) Control concrete specimen

Fig. 10 Microstructure and ITZ

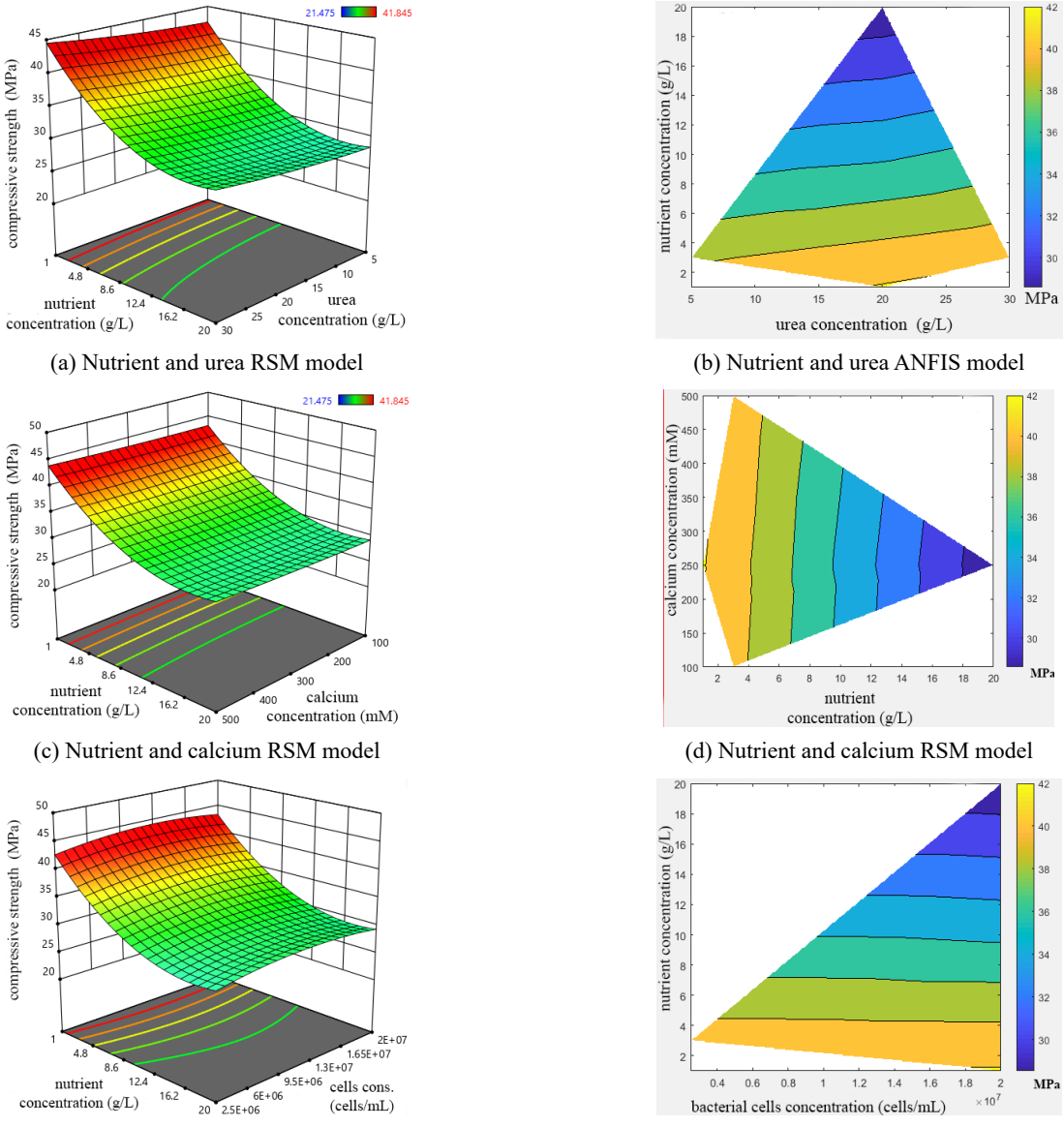

(a) Nutrient and urea RSM model (b) Nutrient and urea ANFIS model

(c) Nutrient and calcium RSM model (d) Nutrient and calcium RSM model

(e) Nutrient and bacterial cells RSM model (f) Nutrient and bacterial cells RSM model

Fig. 11 Evolution of concrete strength due to the interaction between nutrient and other input variables (urea, calcium and bacterial cells)

region- 255). In contrast, the generated X-rays were highly absorbed in a highly dense concrete, and thus, created a bright region in the CT image. According to the three phases of the concrete, the aggregate was denser than the others (C-S-H and ITZ). In addition, the porosity of the cement paste (gel) was lesser than that of the ITZ. Therefore, the high level of brightness represented the aggregate, while the dark colour represented the defect and pores in both the cement gel and ITZ. For simplification, the density of the concrete was represented by different colure counter according to its value in order to simply analyse the variation and location of the porosity in the present study. For example, Figs. 9(a) and (b) show the colour counter distribution of the porosity of both bacterial and control specimens in which the pink region represents the dense concrete and the porous reign was represented by the red colour. It can be seen that the majority of the pink colour is located and distributed in the bacterial concrete skin (5 mm from the concrete surface), while the pink area was limited in the control skin. Therefore, it can be inferred that the percentage of the pores significantly reduced in the bacterial concrete skin compared to that of the control skin which was attributed to the microbial precipitation of calcium carbonate that filled the pores and defects.

In the same context, Figs. 10(a) and (b) illustrate the microstructure of both the bacterial and control specimens. It can be clearly seen that the area of the pores of the bacterial concrete, which was represented by red colour, was lesser than the control one specifically, at the cement gel. While, the pores of both bacterial and control concrete was almost close at the ITZ. This is because of the morphology and composition of the ITZ in which it differs in comparison to that of the cement paste. Specifically, the ITZ is distinguished by a high concentration of calcium hydroxide (Xu *et al*. 2017). Therefore, the ITZ of bacterial concrete was somewhat smaller than the control specimens due to the high pH that might hinder the bacterial activity. Specifically, the thickness of the ITZ of bacterial concrete was found to be within 40 μm compared to that of the control concrete (50 μm). This finding was consistent with a study by Mukharjee and Barai (2014) who stated that the ITZ could be found around the aggregate and had a thickness in the range of 30 to 50 μm. In addition, they concluded that the hardness value was constant and larger at the cement paste.

From another point of view, it was also interesting to note that the size of the pores was classified according to their size. Based on the study of Zhang *et al*. (2018), three

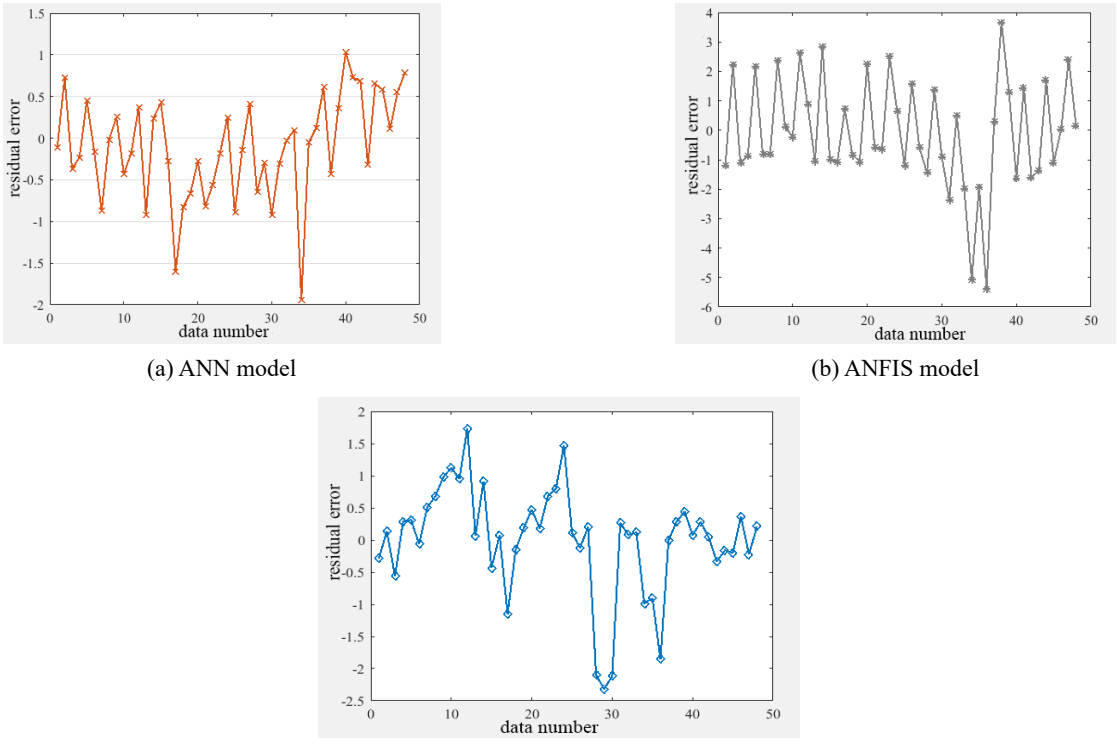

(a) ANN model

(b) ANFIS model

(c) RSM model

Fig. 12 Comparison between residual errors distribution obtained from the three developed models

Table 2 Statistical analysis results

Model	MSE	RMSE	R	R^2	R^2_{adj}	MPE%	RAE	RRSE
RSM	0.704	0.839	0.973	0.972	0.970	1.678	0.131	0.165
ANN	0.628	0.793	0.986	0.985	0.983	1.508	0.11	0.121
ANFIS	0.616	0.785	0.986	0.986	0.984	1.1	0.09	0.12

levels represented the pores according to their diameter. Gel pores represent the smallest pores with a diameter of less than 10 nm. Gel pores are attributed to the hydration process and they are important, as they play a great role in regard to the porosity and durability aspects. The second level is capillary pores, which can range between 10 nm and 1000 nm. Capillary pores are defined as the original water space, which are not filled by the hydrated cement product. Relatedly, capillary pores can be an important factor for concrete strength aspect. Finally, air voids are regarded as the third level, and they are greater than 1000 nm in size. The two main causes of air voids include inadequate compaction and deliberately entrained air. It should be noted that the resolution of X-rays CT reached up to 20 μm. Therefore, pores or voids, that are lesser than 25 μm, was neglected.

3.3 The interaction parameter on concrete strength

Based on the results, it is found that the nutrient concentration was found to be the main parameter that has interaction with other parameters. In other words, the strength significantly decreased with an increasing of yeast extract as illustrated in the distribution counter of the concrete strength even with increasing the concentration of the other parameters. For example, the evolution of the compressive strength of the bacterial concrete as a function of nutrient and urea concentration was represented by colour counter distribution as shown in Figs. 11(a) and (b). It can be seen that the strength decreased with an increase in nutrient concentration even with an increase the urea concentration. This result is very close to the relationship between calcium and nutrient concertation as shown in Figs. 11(c) and (d). In the same context, despite the great importance of bacterial cells concentration on the strength improvement, increasing nutrient negatively affect the strength gain (Figs. 11(e) and (f)). It can be concluded that nutrient does not have any positive role in the precipitation of calcium carbonate inside the concrete matrix. In this present study, this fact was also demonstrated by the X-rays CT images, in which the percentage of the bacterial concrete pores was lesser than that of the control specimen without bacteria. In particular, the decreasing of the concrete pores was observed near the concrete skin. Indeed, by improving the microstructure of the concrete, its strength would also increase. Another reason for strength improvement was that the bacterial cells acted as a nucleation site for calcium ions due to their negative charge. As a result, the bacteria cells themselves filled the micropores inside the concrete matrix.

3.4 Comparison and validation of RSM, ANFIS and ANN models

3.4.1 Comparison of RSM, ANFIS and ANN models

In the present study, the accuracy and performance of the developed models were compared and evaluated using several statistical indicators after finding the best data parameters, as discussed in section 3.4.1. Based on the statistical analysis (Table 2), it is evident that the RSM, ANIFS and ANN models could efficiently predict the compressive strength of concrete. However, Machine learning models (ANN and ANFIS) showed a clear superiority compared to that of the RSM model.

For example, according to Shahmansouri *et al*. (2019), both the actual and predicted results can be considered close results if R^2 is greater than 0.7. In addition, the accuracy of the generated model is improved when it approaches 1. In the same context, when the correlation coefficients (R) was greater than 0.8, the accuracy between the actual and predicted results was achieved. Therefore, our proposed models could be regarded as an accurate model for predicting the compressive strength of bacterial concrete. This is because the R^2, R and adj. R^2 were found to be greater than 0.9 for all models. Such result is an important indicator in regard to the fitness level between the actual and predicted results of the proposed model. Similarly, MSE, RMSE, MPE, RAE and RRSE were also considered to evaluate the efficiency of the models. Based on the results, it can be inferred that the generated models had a minimum error. These indicators values are also regarded as a prove to value the models.

In the same context, the distribution of the residuals error was also taken into account to check the adequacy of the models. This is because a high number of R^2 does not always mean that the generated model is accurate (Hammoudi *et al*. 2019). Therefore, Fig. 12 present the residual error that obtained from the predicted and actual results. It is found that variations of the residuals are regular and small for ANN and ANFIS model compared to that of the RSM model.

4. Conclusions

Bacteria-based self-healing concrete has been recognised as a sustainable strategy to improve concrete properties. However, efforts to optimise the involved parameters are still in demand. In the present study, both experimentally and predictive models using machine learning and RSM were taken into account in order to assess the compressive strength of bacterial concrete incorporating new bacterial species. In particular, a 58 experimental test data were considered under different concentrations of the influential factors. Moreover, the X-rays computed microtomography (CT) technique was also utilised in order to examine and evaluate the micro-voids variation in the bacterial and control concrete microstructure. Based on both the predicted and actual results, the highest enhancement of bacterial concrete strength was 16% higher than the control specimen at optimum concentrations of urea (20 g/L), calcium nitrate tetrahydrate (250 mM), nutrient (3 g/L) and bacterial cells concentration (2×10^7 cells/mL). In addition, the improvement of the bacterial concrete microstructure was clearly observed at the concrete skin (i.e., 5 mm from the concrete surface). For the same regards, the ANFIS, ANN and RSM models proved their ability to accurately predict the compressive strength of bacterial concrete in which the percentage error RMSE and the adjusted determination coefficient were (0.616, 0.628, 0.704) and (0.984, 0.983,

0.97) respectively.

Acknowledgments

The authors acknowledge full gratitude to Universiti Tun Hussein Onn Malaysia (UTHM) and Ministry of Higher Education through fundamental research grant scheme VOT. NO. FRGS /1/2018/TK01/UTHM/02/3. In addition, this research activity was also supported and funded by Malaysian Technical University Network (MTUN) Grant Vot K122 and Industry Grant PLUS BERHAD (M007). Indeed, the authors would like to thank their support and cooperation in this research. Moreover, the authors extend their thanks to Shimadzu Corporation, Alex Corporation (M) Sdn Bhd (KS Wong) and Volume Graphic Software for their assistance and collaboration during the analysis of the X-Ray CT imaging using Shimadzu Inspection System.

References

Abubakar, A.U., Akcaoglu, T. and Marar, K. (2018), "P-value significance level test for high-performance steel fiber concrete (HPSFC)", *Comput. Concrete, Int. J.*, **21**(5), 485-493. https://doi.org/10.12989/cac.2018.21.5.485

Al-Mughanam, T., Aldhyani, T.H., AlSubari, B. and Al-Yaari, M. (2020), "Modeling of Compressive Strength of Sustainable Self-Compacting Concrete Incorporating Treated Palm Oil Fuel Ash Using Artificial Neural Network", *Sustainability*, **12**(22), 9322. https://doi.org/10.3390/su12229322

Alabduljabbar, H., Huseien, G.F., Sam, A.R.M., Alyouef, R., Algaifi, H.A. and Alaskar, A. (2020), "Engineering Properties of Waste Sawdust-Based Lightweight Alkali-Activated Concrete: Experimental Assessment and Numerical Prediction", *Materials*, **13**(23), 5490. https://doi.org/10.3390/ma13235490

Algaifi, H.A., Bakar, S.A., Sam, A.R.M., Abidin, A.R.Z., Shahir, S. and AL-Towayti, W.A.H. (2018), "Numerical modeling for crack self-healing concrete by microbial calcium carbonate", *Constr. Build. Mater.*, **189**, 816-824. https://doi.org/10.1016/j.conbuildmat.2018.08.218

Algaifi, H.A., Bakar, S.A., Sam, A.R.M., Ismail, M., Abidin, A.R.Z., Shahir, S. and Altowayti, W.A.H. (2020), "Insight into the role of microbial calcium carbonate and the factors involved in self-healing concrete", *Constr. Build. Mater.*, **254**, 119258. https://doi.org/10.1016/j.conbuildmat.2020.119258

Algaifi, H.A., Bakar, S.A., Alyousef, R., Sam, A.R.M., Ibrahim, M.W., Shahidan, S., Ibrahim, M. and Salami, B.A. (2021), "Bio-inspired self-healing of concrete cracks using new B. pseudomycoides species", *J. Mater. Res. Technol.*, **12**(5-6), 967-981. https://doi.org/10.1016/j.jmrt.2021.03.037

Alkroosh, I.S. and Sarker, P.K. (2019), "Prediction of the compressive strength of fly ash geopolymer concrete using gene expression programming", *Comput. Concrete, Int. J.*, **24**(4), 295-302. https://doi.org/10.12989/cac.2019.24.4.295

Alshalif, A.F., Irwan, J., Othman, N., Al-Gheethi, A., Shamsudin, S. and Nasser, I.M. (2021), "Optimisation of carbon dioxide sequestration into bio-foamed concrete bricks pores using Bacillus tequilensis", *J. CO2 Utiliz.*, **44**, 101412. https://doi.org/10.1016/j.jcou.2020.101412

Altowayti, W.A.H., Algaifi, H.A., Bakar, S.A. and Shahir, S. (2019), "The adsorptive removal of As (III) using biomass of arsenic resistant Bacillus thuringiensis strain WS3: characteristics and modelling studies", *Ecotoxicol. Environ. Safety*, **172**, 176-185. https://doi.org/10.1016/j.ecoenv.2019.01.067

Awolusi, T.F., Oke, O.L., Akinkurolere, O.O. and Atoyebi, O.D. (2019), "Comparison of response surface methodology and hybrid-training approach of artificial neural network in modelling the properties of concrete containing steel fibre extracted from waste tyres", *Cogent Eng.*, **6**(1), 1649852. https://doi.org/10.1080/23311916.2019.1649852

Bahiraei, M., Mazaheri, N. and Hosseini, S. (2020), "Neural network modeling of thermo-hydraulic attributes and entropy generation of an ecofriendly nanofluid flow inside tubes equipped with novel rotary coaxial double-twisted tape", *Powder Technology*, **369**, 162-175. https://doi.org/10.1016/j.powtec.2020.05.014

Balam, N.H., Mostofinejad, D. and Eftekhar, M. (2017), "Effects of bacterial remediation on compressive strength, water absorption, and chloride permeability of lightweight aggregate concrete", *Constr. Build. Mater.*, **145**, 107-116. https://doi.org/10.1016/j.conbuildmat.2017.04.003

Bundur, Z.B., Kirisits, M.J. and Ferron, R.D. (2015), "Biomineralized cement-based materials: Impact of inoculating vegetative bacterial cells on hydration and strength", *Cem. Concrete Res.*, **67**, 237-245. https://doi.org/10.1016/j.cemconres.2014.10.002

Bundur, Z.B., Amiri, A., Ersan, Y.C., Boon, N. and De Belie, N. (2017), "Impact of air entraining admixtures on biogenic calcium carbonate precipitation and bacterial viability", *Cem. Concrete Res.*, **98**, 44-49. https://doi.org/10.1016/j.cemconres.2017.04.005

Dao, D.V., Ly, H.-B., Trinh, S.H., Le, T.-T. and Pham, B.T. (2019), "Artificial intelligence approaches for prediction of compressive strength of geopolymer concrete", *Materials*, **12**(6), 983. https://doi.org/10.3390/ma12060983

Dutta, S., Samui, P. and Kim, D. (2018), "Comparison of machine learning techniques to predict compressive strength of concrete", *Comput. Concrete, Int. J.*, **21**(4), 463-470. https://doi.org/10.12989/cac.2018.21.4.463

Golafshani, E.M., Behnood, A. and Arashpour, M. (2020), "Predicting the compressive strength of normal and High-Performance Concretes using ANN and ANFIS hybridized with Grey Wolf Optimizer", *Constr. Build. Mater.*, **232**, 117266. https://doi.org/10.1016/j.conbuildmat.2019.117266

Hammoudi, A., Moussaceb, K., Belebchouche, C. and Dahmoune, F. (2019), "Comparison of artificial neural network (ANN) and response surface methodology (RSM) prediction in compressive strength of recycled concrete aggregates", *Constr. Build. Mater.*, **209**, 425-436. https://doi.org/10.1016/j.conbuildmat.2019.03.119

Huseien, G.F., Sam, A.R.M., Algaifi, H.A. and Alyouef, R. (2021), "Development of a sustainable concrete incorporated with effective microorganism and fly Ash: Characteristics and modeling studies", *Constr. Build. Mater.*, **285**, 122899. https://doi.org/10.1016/j.conbuildmat.2021.122899

Jafari, S. and Mahini, S.S. (2017), "Lightweight concrete design using gene expression programing", *Constr. Build. Mater.*, **139**, 93-100. https://doi.org/10.1016/j.conbuildmat.2021.122899

Jakubovskis, R., Jankutė, A., Urbonavičius, J. and Gribniak, V. (2020), "Analysis of mechanical performance and durability of self-healing biological concrete", *Constr. Build. Mater.*, **260**, 119822. https://doi.org/10.1016/j.conbuildmat.2020.119822

Jena, S., Basa, B., Panda, K.C. and Sahoo, N.K. (2020), "Impact of Bacillus subtilis bacterium on the properties of concrete", *Mater Today Proc.* https://doi.org/10.1016/j.matpr.2020.03.129

Kathirvel, P. and Kaliyaperumal, S.R.M. (2017), "Probabilistic modeling of geopolymer concrete using response surface methodology", *Comput. Concrete, Int. J.*, **19**(6), 737-744. https://doi.org/10.12989/cac.2017.19.6.737

Liu, Q.-f., Iqbal, M.F., Yang, J., Lu, X.-y., Zhang, P. and Rauf, M. (2021), "Prediction of chloride diffusivity in concrete using artificial neural network: Modelling and performance evaluation", *Constr. Build. Mater.*, **268**, 121082. https://doi.org/10.1016/j.conbuildmat.2020.121082

Ma, X., Foong, L.K., Morasaei, A., Ghabussi, A. and Lyu, Z. (2020), "Swarm-based hybridizations of neural network for predicting the concrete strength", *Smart Struct. Syst.*, *Int. J.*, **26**(2), 241-251. https://doi.org/10.12989/sss.2020.26.2.241

Mahdinia, S., Eskandari-Naddaf, H. and Shadnia, R. (2019), "Effect of cement strength class on the prediction of compressive strength of cement mortar using GEP method", *Constr. Build. Mater.*, **198**, 27-41. https://doi.org/10.1016/j.conbuildmat.2018.11.265

Mahmud, M.Z.H., Hassan, N.A., Hainin, M.R. and Ismail, C.R. (2017), "Microstructural investigation on air void properties of porous asphalt using virtual cut section", *Constr. Build. Mater.*, **155**, 485-494. https://doi.org/10.1016/j.conbuildmat.2017.08.103

Mondal, S. and Ghosh, A.D. (2019), "Review on microbial induced calcite precipitation mechanisms leading to bacterial selection for microbial concrete", *Constr. Build. Mater.*, **225**, 67-75. https://doi.org/10.1016/j.conbuildmat.2019.07.122

Mousavi, S.M., Aminian, P., Gandomi, A.H., Alavi, A.H. and Bolandi, H. (2012), "A new predictive model for compressive strength of HPC using gene expression programming", *Adv. Eng. Software*, **45**(1), 105-114. https://doi.org/10.1016/j.advengsoft.2011.09.014

Mukharjee, B.B. and Barai, S.V. (2014), "Influence of incorporation of nano-silica and recycled aggregates on compressive strength and microstructure of concrete", *Constr. Build. Mater.*, **71**, 570-578. https://doi.org/10.1016/j.conbuildmat.2014.08.040

Muthuraj, M. (2019), "Prediction of compressive strength of bacteria incorporated geopolymer concrete by using ANN and MARS", *Struct. Eng. Mech.*, *Int. J.*, **70**(6), 671-681. https://doi.org/10.12989/sem.2019.70.6.671

Naderpour, H. and Mirrashid, M. (2020), "Estimating the compressive strength of eco-friendly concrete incorporating recycled coarse aggregate using neuro-fuzzy approach", *J. Clean. Prod.*, 121886. https://doi.org/10.1016/j.jclepro.2020.121886

Nain, N., Surabhi, R., Yathish, N., Krishnamurthy, V., Deepa, T. and Tharannum, S. (2019), "Enhancement in strength parameters of concrete by application of Bacillus bacteria", *Constr. Build. Mater.*, **202**, 904-908. https://doi.org/10.1016/j.conbuildmat.2019.01.059

Nathaniel, O., Sam, A.R.M., Lim, N.H.A.S., Adebisi, O. and Abdulkareem, M. (2020), "Biogenic approach for concrete durability and sustainability using effective microorganisms: A review", *Constr. Build. Mater.*, **261**, 119664. https://doi.org/10.1016/j.conbuildmat.2020.119664

Nematzadeh, M., Shahmansouri, A.A. and Zabihi, R. (2021), "Innovative models for predicting post-fire bond behavior of steel rebar embedded in steel fiber reinforced rubberized concrete using soft computing methods", In: *Structures*, Vol. 31, pp. 1141-1162.

Nguyen, T.H., Ghorbel, E., Fares, H. and Cousture, A. (2019), "Bacterial self-healing of concrete and durability assessment", *Cem. Concrete Compos.*, **104**, 103340. https://doi.org/10.1016/j.cemconcomp.2019.103340

Nigdeli, S.M. and Bekdas, G. (2013), "Optimum tuned mass damper design for preventing brittle fracture of RC buildings", *Smart Struct. Syst.*, *Int. J.*, **12**(2), 137-155. https://doi.org/10.12989/sss.2013.12.2.137

Nosrati, A., Zandi, Y., Shariati, M., Khademi, K., Aliabad, M.D., Marto, A., Mu'azu, M., Ghanbari, E., Mahdizadeh, M. and Shariati, A. (2018), "Portland cement structure and its major oxides and fineness", *Smart Struct. Syst.*, *Int. J.*, **22**(4), 425-432. https://doi.org/10.12989/sss.2018.22.4.425

Okwadha, G.D. and Li, J. (2010), "Optimum conditions for microbial carbonate precipitation", *Chemosphere*, **81**(9), 1143-1148. https://doi.org/10.1016/j.chemosphere.2010.09.066

Onat, O. and Celik, E. (2017), "An integral based fuzzy approach to evaluate waste materials for concrete", *Smart Struct. Syst.*, *Int. J.*, **19**(3), 323-333. https://doi.org/10.12989/sss.2017.19.3.323

Perumal, R. and Prabakaran, V. (2020), "Estimating the compressive strength of HPFRC containing metallic fibers using statistical methods and ANNs", *Adv. Concrete Constr.*, *Int. J.*, **10**(6), 479-488. https://doi.org/10.12989/acc.2020.10.6.479

Prasad, B.R., Eskandari, H. and Reddy, B.V. (2009), "Prediction of compressive strength of SCC and HPC with high volume fly ash using ANN", *Constr. Build. Mater.*, **23**(1), 117-128. https://doi.org/10.1016/j.conbuildmat.2008.01.014

Qian, C., Wang, J., Wang, R. and Cheng, L. (2009), "Corrosion protection of cement-based building materials by surface deposition of $CaCO_3$ by *Bacillus pasteurii*", *Mater. Sci. Eng.: C*, **29**(4), 1273-1280. https://doi.org/10.1016/j.msec.2008.10.025

Reddy, B.M.S. and Revathi, D. (2019), "An experimental study on effect of Bacillus sphaericus bacteria in crack filling and strength enhancement of concrete", *Materials Today: Proceedings*, **19**(2), 803-809. https://doi.org/10.1016/j.matpr.2019.08.135

Sadowski, L., Nikoo, M. and Nikoo, M. (2018), "Concrete compressive strength prediction using the imperialist competitive algorithm", *Comput. Concrete*, *Int. J.*, **22**(4), 355-363. https://doi.org/10.12989/cac.2018.22.4.355

Scrivener, K., Füllmann, T., Gallucci, E., Walenta, G. and Bermejo, E. (2004), "Quantitative study of Portland cement hydration by X-ray diffraction/Rietveld analysis and independent methods", *Cem. Concrete Res.*, **34**(9), 1541-1547. https://doi.org/10.1016/j.cemconres.2004.04.014

Shaban, W.M., Yang, J., Elbaz, K., Xie, J. and Li, L. (2021), "Fuzzy-metaheuristic ensembles for predicting the compressive strength of brick aggregate concrete", *Resour. Conserv. Recycl.*, **169**, 105443. https://doi.org/10.1016/j.resconrec.2021.105443

Shaheen, N., Khushnood, R.A., Khaliq, W., Murtaza, H., Iqbal, R. and Khan, M.H. (2019), "Synthesis and characterization of bio-immobilized nano/micro inert and reactive additives for feasibility investigation in self-healing concrete", *Constr. Build. Mater.*, **226**, 492-506. https://doi.org/10.1016/j.conbuildmat.2019.07.202

Shahmansouri, A.A., Bengar, H.A. and Jahani, E. (2019), "Predicting compressive strength and electrical resistivity of eco-friendly concrete containing natural zeolite via GEP algorithm", *Constr. Build. Mater.*, **229**, 116883. https://doi.org/10.1016/j.conbuildmat.2019.116883

Shahmansouri, A.A., Yazdani, M., Ghanbari, S., Bengar, H.A., Jafari, A. and Ghatte, H.F. (2020), "Artificial neural network model to predict the compressive strength of eco-friendly geopolymer concrete incorporating silica fume and natural zeolite", *J. Clean. Prod.*, **279**, 123697. https://doi.org/10.1016/j.jclepro.2020.123697

Shahmansouri, A.A., Bengar, H.A. and AzariJafari, H. (2021a), "Life cycle assessment of eco-friendly concrete mixtures incorporating natural zeolite in sulfate-aggressive environment", *Constr. Build. Mater.*, **268**, 121136. https://doi.org/10.1016/j.conbuildmat.2020.121136

Shahmansouri, A.A., Nematzadeh, M. and Behnood, A. (2021b), "Mechanical properties of GGBFS-based geopolymer concrete incorporating natural zeolite and silica fume with an optimum design using response surface method", *J. Build. Eng.*, **36**,

102138. https://doi.org/10.1016/j.jobe.2020.102138
Shariati, M., Mafipour, M.S., Haido, J.H., Yousif, S.T., Toghroli, A., Trung, N.T. and Shariati, A. (2020a), "Identification of the most influencing parameters on the properties of corroded concrete beams using an Adaptive Neuro-Fuzzy Inference System (ANFIS)", *Steel Compos. Struct., Int. J.*, **34**(1), 155-170. https://doi.org/10.12989/scs.2020.34.1.155
Shariati, M., Mafipour, M.S., Mehrabi, P., Ahmadi, M., Wakil, K., Trung, N.T. and Toghroli, A. (2020b), "Prediction of concrete strength in presence of furnace slag and fly ash using Hybrid ANN-GA (Artificial Neural Network-Genetic Algorithm)", *Smart Struct. Syst., Int. J.*, **25**(2), 183-195. https://doi.org/10.12989/sss.2020.25.2.183
Shirkhani, A., Davarnia, D. and Azar, B.F. (2019), "Prediction of bond strength between concrete and rebar under corrosion using ANN", *Comput. Concrete, Int. J.*, **23**(4), 273-279. https://doi.org/10.12989/cac.2019.23.4.273
Siddique, R., Jameel, A., Singh, M., Barnat-Hunek, D., Aït-Mokhtar, A., Belarbi, R. and Rajor, A. (2017), "Effect of bacteria on strength, permeation characteristics and micro-structure of silica fume concrete", *Constr. Build. Mater.*, **142**, 92-100. https://doi.org/10.1016/j.conbuildmat.2017.03.057
Snoeck, D., Dewanckele, J., Cnudde, V. and De Belie, N. (2016), "X-ray computed microtomography to study autogenous healing of cementitious materials promoted by superabsorbent polymers", *Cem. Concrete Compos.*, **65**, 83-93. https://doi.org/10.1016/j.cemconcomp.2015.10.016
Sokhansefat, G., Moradian, M., Finnell, M., Behravan, A., Ley, M.T., Lucero, C. and Weiss, J. (2020), "Using X-ray computed tomography to investigate mortar subjected to freeze-thaw cycles", *Cem. Concrete Compos.*, **108**, 103520. https://doi.org/10.1016/j.cemconcomp.2020.103520
Soto-Pérez, L., Lopez, V. and Hwang, S.S. (2015), "Response Surface Methodology to optimize the cement paste mix design: Time-dependent contribution of fly ash and nano-iron oxide as admixtures", *Mater. Des.*, **86**, 22-29. https://doi.org/10.1016/j.matdes.2015.07.049
Su, Y., Feng, J., Jin, P. and Qian, C. (2019), "Influence of bacterial self-healing agent on early age performance of cement-based materials", *Constr. Build. Mater.*, **218**, 224-234. https://doi.org/10.1016/j.conbuildmat.2019.05.077
Topcu, I.B. and Sarıdemir, M. (2008), "Prediction of compressive strength of concrete containing fly ash using artificial neural networks and fuzzy logic", *Computat. Mater. Sci.*, **41**(3), 305-311. https://doi.org/10.1016/j.commatsci.2007.04.009
Valipour, M., Yekkalar, M., Shekarchi, M. and Panahi, S. (2014), "Environmental assessment of green concrete containing natural zeolite on the global warming index in marine environments", *J. Clean. Prod.*, **65**, 418-423. https://doi.org/10.1016/j.jclepro.2013.07.055
Wang, J., Jonkers, H.M., Boon, N. and De Belie, N. (2017), "Bacillus sphaericus LMG 22257 is physiologically suitable for self-healing concrete", *Appl. Microbiol. Biotechnol.*, **101**(12), 5101-5114. https://doi.org/10.1007/s00253-017-8260-2
Wu, M., Hu, X., Zhang, Q., Cheng, W., Xue, D. and Zhao, Y. (2020), "Application of bacterial spores coated by a green inorganic cementitious material for the self-healing of concrete cracks", *Cem. Concrete Compos.*, 103718. https://doi.org/10.1016/j.cemconcomp.2020.103718
Xu, J., Wang, B. and Zuo, J. (2017), "Modification effects of nanosilica on the interfacial transition zone in concrete: A multiscale approach", *Cem. Concrete Compos.*, **81**, 1-10. https://doi.org/10.1016/j.cemconcomp.2017.04.003
Zhang, J.L., Wu, R.S., Li, Y.M., Zhong, J.Y., Deng, X., Liu, B., Han, N.X. and Xing, F. (2016), "Screening of bacteria for self-healing of concrete cracks and optimization of the microbial calcium precipitation process", *Appl. Microbiol. Biotechnol.*, **100**(15), 6661-6670. https://doi.org/10.1007/S00253-016-7382-2
Zhang, J., Bian, F., Zhang, Y., Fang, Z., Fu, C. and Guo, J. (2018), "Effect of pore structures on gas permeability and chloride diffusivity of concrete", *Constr. Build. Mater.*, **163**, 402-413. https://doi.org/10.1016/j.conbuildmat.2017.12.111
Zhang, J., Li, D. and Wang, Y. (2020), "Predicting uniaxial compressive strength of oil palm shell concrete using a hybrid artificial intelligence model", *J. Build. Eng.*, **30**, 101282. https://doi.org/10.1016/j.jobe.2020.101282
Zhao, Y., Moayedi, H., Bahiraei, M. and Foong, L.K. (2020), "Employing TLBO and SCE for optimal prediction of the compressive strength of concrete", *Smart Struct. Syst., Int. J.*, **26**(6), 753-763. http://doi.org/10.12989/sss.2020.26.6.753
Zhao, Y., Bai, C., Xu, C. and Foong, L.K. (2021a), "Efficient metaheuristic-retrofitted techniques for concrete slump simulation", *Smart Struct. Syst., Int. J.*, **27**(5), 745-759. http://doi.org/10.12989/sss.2021.27.5.745
Zhao, Y., Zhong, X. and Foong, L.K. (2021b), "Predicting the splitting tensile strength of concrete using an equilibrium optimization model", *Steel Compos. Struct., Int. J.*, **39**(1), 81-93. https://doi.org/10.12989/scs.2021.39.1.081

CC